Research Article | Vol. 31, No. 22 / 23 Oct 2023 / Optics Express 36293
Optics EXPRESS

Analysis of size-dependent optoelectronic properties of red AlGaInP micro-LEDs

KAILI FAN,[1,2,3,4] KAIFENG ZHENG,[1,3,4] JINGUANG LV,[1,3,4] BAIXUAN ZHAO,[1,3,4] YINGZE ZHAO,[1,3,4] YUPENG CHEN,[1,3,4] YUXIN QIN,[1,3,4] QIANG WANG,[1,3,4] WEIBIAO WANG,[1,3,4,5] AND JINGQIU LIANG[1,3,4,6]

[1]*Changchun Institute of Optics, Fine Mechanics and Physics, Chinese Academy of Sciences, Changchun, Jilin 130033, China*
[2]*University of Chinese Academy of Sciences, Beijing 100049, China*
[3]*State Key Laboratory of Applied Optics, Changchun, Jilin 130033, China*
[4]*Key Laboratory of Optical System Advanced Manufacturing Technology, Chinese Academy of Sciences, Changchun, Jilin 130033, China*
[5]*wangwb@ciomp.ac.cn*
[6]*liangjq@ciomp.ac.cn*

Abstract: We have theoretically investigated the size-dependent optoelectronic properties of InGaP/AlGaInP-based red micro-LEDs through an electro-optical-thermal coupling model. The model considers thermal effects due to current crowding near the electrodes, non-thermal efficiency droop due to electron leakage, and etch defects on the LED sidewall. Sidewall defects reduce the carrier concentration at the light-emitting surface's edge and exacerbate the current crowding effect. In addition, p-side electron leakage at high current densities is the leading cause of the efficiency droop of AlGaInP LEDs. In contrast, the effect of temperature on the overall efficiency degradation of LEDs is even more significant.

1. Introduction

Currently, high-efficiency micro-LED devices based on InGaN and AlGaInP have a wide range of promising applications, such as high-resolution micro-displays [1–3], biosensing [4], wearable devices [5,6], augmented reality and virtual reality [7,8], visible light communication [9], and so on. One of the significant challenges for micro-LED devices, which require smaller and smaller chip sizes and pixel pitches, is high resolution and high pixel density technologies [10]. However, as chip size is reduced to the micron level, the external quantum efficiency (EQE) of LEDs decreases dramatically due to sidewall etch defects that become non-radiative recombination centers during pixel separation, thus reducing the internal quantum efficiency (IQE) [11]. Previous studies [12–15] have also reported the relationship between the optoelectronic properties and chip size of AlGaInP red micro-LEDs. However, these studies mainly focused on analyzing and discussing the experimental results, and the physical mechanisms by which defects caused by the fabrication process affect device efficiency are not yet precise. Recently, Zhang et al. [16,17] numerically investigated the impact of surface recombination on the optoelectronic performance of GaN-based blue LEDs by TCAD simulator, and they did not consider the self-heating effect. However, AlGaInP LEDs are more sensitive to temperature, and nitride and phosphide LEDs have different material properties and efficiency droop mechanisms. Although III-nitride red micro-LEDs have thermal stability and monolithic integration potential, their low efficiency, wide emission bandwidth, and drive current wavelength shift remain major challenges for display applications [18]. In contrast, conventional AlGaInP red LEDs exhibit excellent efficiency and optical properties such as narrow emission bandwidth. On the other hand, the absence of internal electric fields associated with polarization makes AlGaInP LEDs a potential choice for

#503024 https://doi.org/10.1364/OE.503024
Journal © 2023 Received 10 Aug 2023; revised 18 Sep 2023; accepted 20 Sep 2023; published 13 Oct 2023

Optics EXPRESS

micro-LED visible light communication data transmission. However, size effects limit the use of AlGaInP micro-LEDs because their efficiency decreases significantly with decreasing device size. In addition, there is an inherent thermal degradation in AlGaInP micro-LEDs due to the direct-indirect bandgap transition and carrier overflow, leading to instability at high temperatures and reduced EQE efficiency [19]. Therefore, it is necessary to elucidate the physical mechanisms of the size-dependent optoelectronic properties of AlGaInP-based red LEDs to optimize the device structure and fully mitigate the effects of the fabrication process.

In this study, we theoretically investigate the dimensional trends of InGaP/AlGaInP-based red LEDs to understand better the physical mechanisms underlying the evolution of the optoelectronic properties and efficiency of red LEDs. To this end, we develop an electrical-optical-thermal coupling model [20,21] and consider the interactions between the above phenomena. These results will provide a theoretical basis for optimizing the LED structure to alleviate the size dependence and meet the diverse requirements of future micro-LED devices.

2. Device structures and parameters

The structure and modeling parameters of the InGaP/AlGaInP-based red LED devices are shown in Table 1 and Table 2. The specific structural parameters can be found in the previously published experimental results [22]. To investigate the scaling trend, the size of the LED chip is reduced from 160 μm to 10 μm, and the n-electrode occupancy is kept constant. The width of the damaged area is set to 5 μm [see Table 1], the specific resistance of the p-type ohmic contact is set to 5×10^{-5} Ω cm^2 for all LEDs, and the specific resistance of the n-type ohmic contact is set to 5×10^{-3} Ω cm^2. The heat sink temperature is set to 300 K to account for the LED model's self-heating effect, and the device's heat dissipation is simulated by a heat transfer coefficient of 10 W/cm^2 K.

Table 1. LED structure (from top to bottom).

Layer	Thickness, nm	Doping, cm^{-3}
n-GaAs	80	5×10^{18}
$In_{0.4}Al_{0.1}GaP$ n-cladding layer	2300	2×10^{18}
$In_{0.4}Al_{0.1}GaP$ n-side SCL layer	111	undoped
10×(6 nm $In_{0.51}GaP$ /11 nm $In_{0.3}Al_{0.2}GaP$) MQW	159	undoped
$In_{0.4}Al_{0.1}GaP$ p-side SCL layer	80	undoped
$In_{0.4}Al_{0.1}GaP$ p-cladding layer	350	3×10^{18}
p-GaP	1500	3×10^{18}

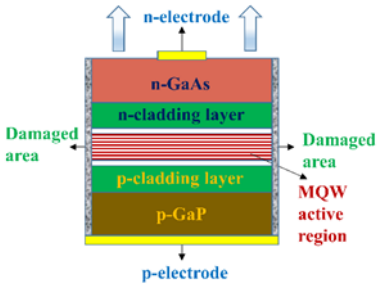

Numerical calculations are performed using the TCAD simulator, and the Block-Newton nonlinear iterative strategy [26] is used to solve the carrier continuity equation, the Poisson's ratio equation, the transport equation, and the displacement current equation under appropriate boundary conditions [27]. The drift-diffusion transport model used in this study considers nonequilibrium carrier injection, non-radiative and radiative recombination, and light emission. The IQE takes into account not only the competition between the radiative and non-radiative recombination channels but also the carrier leakage from the p-n junction region. Mechanisms of electro-thermal conversion include ohmic heating of the material bulk, heating due to the thermalization of nonequilibrium carriers in the p-n junction region, and heating related to the absorption of emitted light in the LED structure as the principal heat source [21]. Specifically, for

Optics EXPRESS

Table 2. LED model parameters.

Device size	Model 1 (no-sidewall defects)	Model 2 (sidewall defects)	Percentage of sidewall damage (Model 1/Model 2)	Auger recombination coefficient [23–25]	SRH Lifetime [23–25]
10μm*10μm	LED A	LED I	0/100%		
20μm*20μm	LED B	LED II	0/50%		
40μm*40μm	LED C	LED III	0/25%	5×10^{-28} cm^6 s^{-1}	5×10^{-9} s^{-1}
80μm*80μm	LED D	LED IV	0/12.5%		
160μm*160μm	LED E	LED V	0/6.25%		

the LED in Model 2, the acceptor trap energy level is adjusted to 0.45 eV below the conduction band, with a trap cross section of 1×10^{-14} cm^2 and a density of 1×10^{16} cm^{-3} [28]. The donor trap energy level is 1.32 eV above the valence band, its density is 1.6×10^{16} cm^{-3}, and the trap capture cross section is 3×10^{-14} cm^2 [29].

3. Results and discussions

3.1. Size-dependent trends in EQE

Figure 1(a) shows the semi-logarithmic current density voltage characteristics of two groups of LEDs. By comparing the two groups of LEDs, it is found that the turn-on voltages of different sizes of LEDs in Model 2 are different. The difference in turn-on voltage for the same-size LEDs in Model 1 and Model 2 is defined as ΔV. As shown in the inset, the smaller the chip size, the larger ΔV appears, owing to the higher current leakage through the lateral surface defects [16]. In Fig. 1(b-c), the variation of EQE and optical power density with the injected current density is calculated for both groups of devices. For Model 1, EQE and optical power density increase due to the better current-spreading effect of the smaller chip size [15]. For Model 2, EQE and optical power density decrease with decreasing device size. Figure 1(d) shows the two main trends of EQE variation with LED size reduction in Model 2: (i) the maximum (peak) EQE decreases, and (ii) the peak current density increases when the maximum EQE is reached. These two trends are consistent with the experimental trends reported in [22,30].

3.2. Thermal effects from current crowding

The local current density distributions of the two groups of LEDs over the active region are compared in Fig. 2(a-b) (all horizontal positions have been normalized for easy comparison, and the horizontal coordinates in the figure are in relative positions). The current distribution of large-size LEDs (above 40 μm) is extremely non-uniform, with a peak current density of more than 1000 A/cm^2 at the n-electrode, indicating strong current crowding, which is greatly improved in small-size LEDs, and it is worth mentioning that this phenomenon is consistent with that of current crowding in InGaN-based LEDs [31–34]. In Model 2, the current density at the edges of all the LEDs' light-emitting surfaces is reduced, making the current crowding effect more severe. Figure 2(c-d) shows the local lattice temperature distributions of the two groups of LEDs. In Model 1, the temperature increases with increasing chip size, and the larger the chip size, the more inhomogeneous the temperature distribution is due to the concentration of current density near n-electrodes, which leads to similar thermal localization and inhomogeneous temperature distribution in the active region.

As can be seen in Fig. 2(c), the temperatures of LED A, LED B, LED C, and LED D are almost the same at different locations on the chip. This is because the simulation model in this study chooses a vertical LED structure, which is consistent with the structure of previously manufactured LED chips. The vertical LED structure adopts a high thermal conductivity silicon

Optics EXPRESS

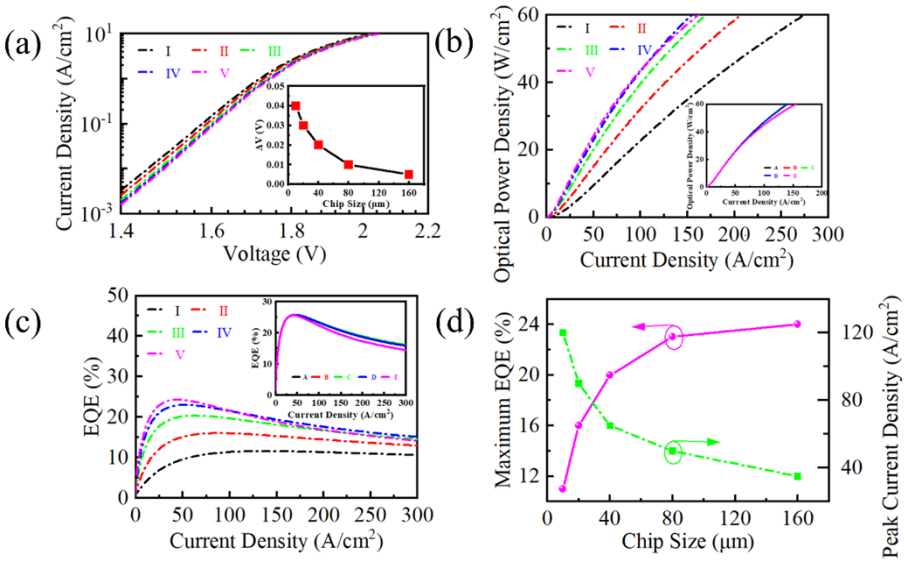

Fig. 1. (a) Semi-logarithmic current density-voltage characteristics for different LEDs in Model 1 and Model 2, with insets showing the defined turn-on voltage difference versus chip size; (b) optical power density in terms of injected current density; (c) EQE in terms of injected current density; (d) maximum EQE in Model 2 and peak current density versus chip size.

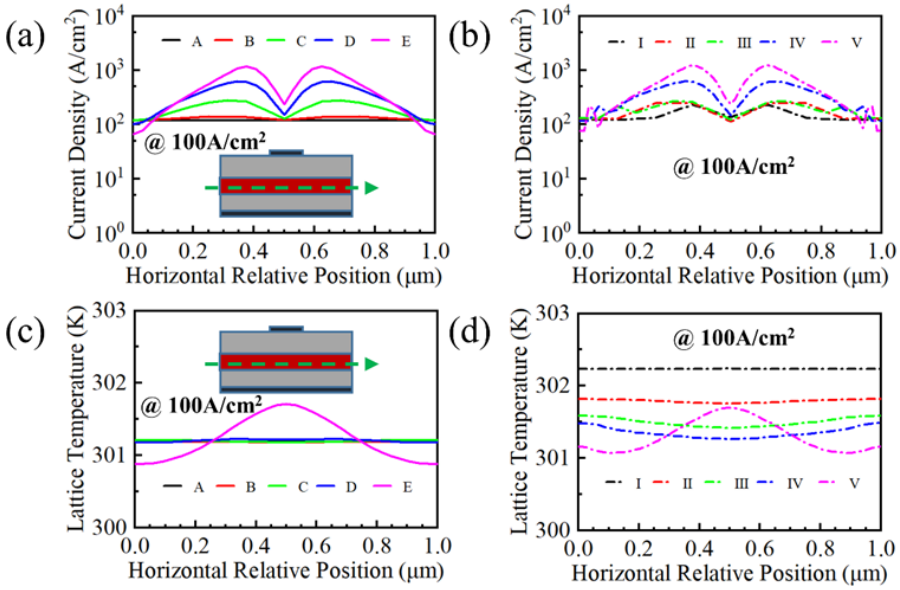

Fig. 2. (a-b) Horizontal current density distribution, (c-d) horizontal lattice temperature distribution in the first quantum well closest to the p-cladding layer for different LEDs in Model 1 and Model 2 at an average current density of about 100 A/cm^2. The inset shows the current and temperature distribution variation with the corresponding position (indicated by the green arrow).

Optics EXPRESS

substrate instead of a GaAs substrate, dramatically improving heat dissipation efficiency. In addition, the two electrodes of the vertical LED chip are located on both sides of the LED epitaxial layer, and through the n-electrode, almost all the current flows vertically through the LED epitaxial layer, and the transverse current is very small, which avoids the local high temperature. Therefore, for small-sized vertical LEDs (<80μm), the problem of localized high temperature caused by current crowding can be effectively improved. On the other hand, due to good heat dissipation, the heat generated by current crowding is effectively dissipated, thus avoiding the localized high temperature caused by heat accumulation. In Model 2, current crowding and leakage are exacerbated by sidewall defects, resulting in a more severe self-heating effect for small-sized LEDs.

3.3. LED Self-heating red shift effect

As shown in Fig. 3(a), the specific thermal resistance increases with LED size due to the chip size-related current crowding effect, leading to more intense self-heating large-sized devices (above 80 μm) [35]. In Model 2, the self-heating effect of small-size LEDs becomes more severe, which is also found in Ref. [36]. This is because small-sized LEDs introduce more defects, leading to more severe current crowding effects and larger leakage currents, while the sidewall defects also enhance the non-radiative recombination, resulting in a stronger self-heating effect for small-sized LEDs. In Fig. 3(b), the self-heating effect increases the lattice temperature, which causes the MQW bandgap to narrow and the peak wavelength to red-shift [37]. When the peak wavelength is red-shifted to 629.4 nm, the bandgap changes faster with increasing temperature. The vertical and horizontal energy band distributions of the 10 μm LED are shown in Fig. 3(c-d), and the energy band distribution changes very little after considering the sidewall defects, indicating that the peak wavelength drift of the red LED is mainly due to the temperature-induced bandgap narrowing. Therefore, it is necessary to analyze the performance changes of LEDs at different lattice temperatures. From Fig. 3(a), it can be seen that for different sizes of LEDs, the maximum temperature rise value due to the self-heating effect is less than 20 K in the current density range of 0-300 A/cm^2. Therefore, we investigated the effect of the lattice temperature on the overall efficiency degradation of EQE in the temperature range of 300-330 K.

3.4. Temperature effects on EQE

Figure 4(a) shows the variation of EQE of LED III in model 2 at different lattice temperatures; with the increase of temperature, the peak EQE decreases at all current densities, and all of them show efficiency droop, and the magnitude of efficiency droop does not increase with the increase of temperature. Therefore, the temperature mainly affects the overall efficiency of the LEDs, and the rise in temperature does not exacerbate the trend of decreasing efficiency. The vertical electron concentration and hole concentration distributions in the active region of the LED are shown in Fig. 4(b-c); with the increase in temperature, the electron concentration of quantum wells increases, the electron concentration of quantum barriers decreases, and the electron concentration of p-side and n-side SCL layers decreases. At the same time, the hole concentration does not change significantly with increasing temperature. By comparing the local recombination rates in the active region, as shown in Fig. 4(d-f), it can be seen that the radiative recombination rate of the LED decreases and the Shockley-Read-Hall (SRH) non-radiative recombination rate as well as the Auger recombination rate increase with the increase in temperature, which leads to a decrease in the peak EQE of the LED. For example, at 315 K, the radiative recombination rate decreases by 60%, the SRH non-radiative recombination rate increases by 100%, and the Auger recombination rate increases by 30%; this is attributed to the low carrier-limiting effect on the MQW structure, which is limited by the small bandgap of the AlGaInP material itself, resulting in easy carrier leakage and a sharp decrease in radiative recombination. On the other hand, the doping sources in the p-type and n-type semiconductor layers on both sides enter into the active

Optics EXPRESS

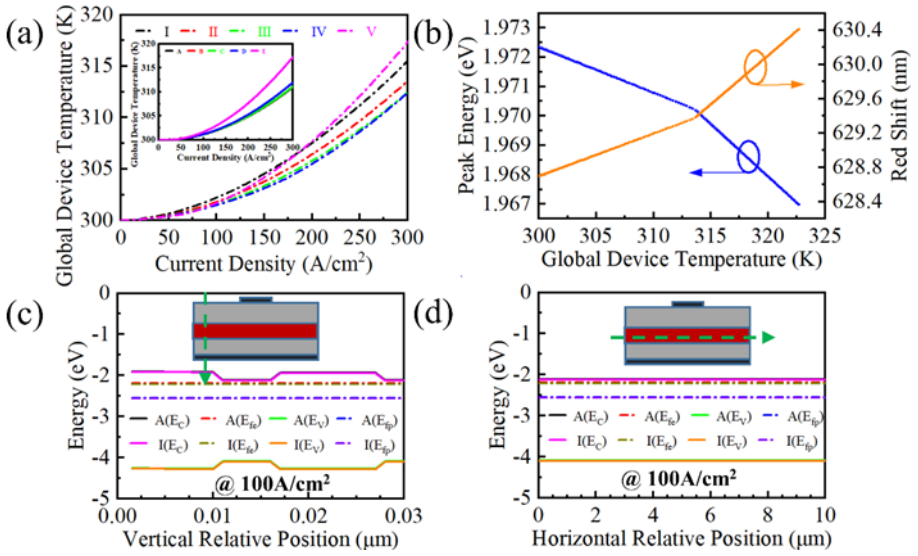

Fig. 3. (a) Variation of global device temperature due to self-heating effect of different LEDs in Model 1 and Model 2 with change of injection current density, (b) variation of MQW bandgap and peak wavelength with temperature, (c) vertical band distribution of LED A and LED I in the first quantum well closest to the p-cladding layer at 2.5 μm from the light-emitting surface edge at an average current density of about 100 A/cm^2, and (d) horizontal band distribution of LED A and LED I in the first quantum well closest to the p-cladding layer at an average current density of about 100 A/cm^2. The inset shows the energy band distribution variation with the corresponding position (indicated by the green arrow).

region, which leads to the formation of non-radiative recombination centers and increases the non-radiative recombination [37]. In conclusion, there is an inherent EQE thermal degradation in AlGaInP devices with increasing temperature, which is attributed to direct-indirect bandgap transition and carrier overflow [18]. Therefore, the epitaxial structure needs to be optimized to increase the critical temperature of EQE thermal degradation in order to mitigate the thermal degradation in AlGaInP devices.

3.5. *P-side electron leakage leading to efficiency droop*

The effect of self-heating on EQE can be reduced by improving the LED structure and heat dissipation effect, but there is still a tendency for EQE efficiency to decrease at high current densities. Therefore, we investigated the effect of p-side electron leakage on the efficiency of AlGaInP LEDs at different current densities. The two models' p-side electron concentrations of different LEDs are shown in Fig. 5(a). The 160 μm LED has the lowest leakage electrons in the p-type GaP layer. However, the presence or absence of sidewall defects does not affect the p-side electron leakage. Taking the 10 μm LED as an example, the electron concentrations of LED C and LED III in the p-cladding and p-GaP layers at different current densities are compared in Fig. 5(b), and it is found that the active region and the electron blocking layer of the LED at higher injection currents enhance the leakage of injected electrons into the p-type GaP layer; this means that the physical effects associated with higher currents push electrons out of the recombination region so that they never have a chance to encounter holes and release photons, which is the root cause of the efficiency droop in red LEDs [38]. As shown in Fig. 5(b-d), there are slight differences in the degree of electron leakage for different sizes of LEDs. Still, the trend

Optics EXPRESS

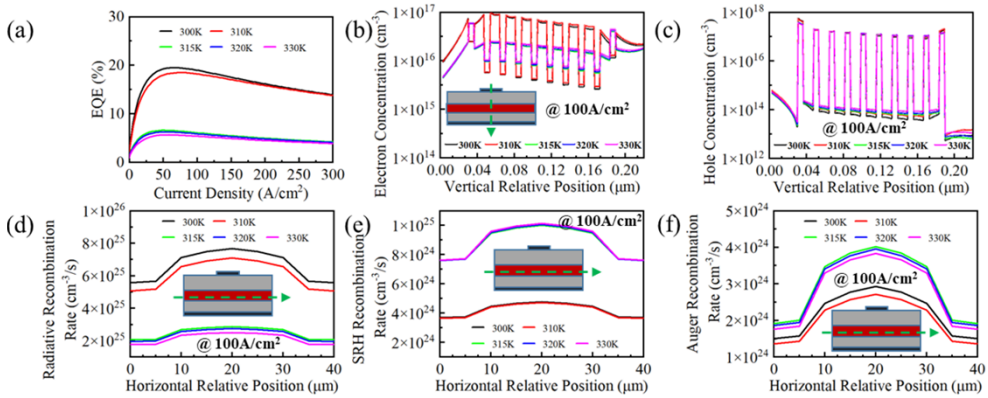

Fig. 4. (a) EQE in terms of injected current density, (b-c) vertical electron concentration and hole concentration distribution in the MQW region at the center of the light-emitting surface at an average current density of about 100 A/cm^2 for LED III at different lattice temperatures; (d) horizontal radiative recombination rate in the first quantum well closest to the p-cladding layer at an average current density of about 100 A/cm^2, (e) horizontal SRH recombination rate and (f) horizontal Auger recombination rate. The inset shows the electron concentration and recombination rate distribution variation with the corresponding position (indicated by the green arrow).

is consistent, with all p-side electron leakage increasing with the increase in drive current density. Therefore, only by fully optimizing the epitaxial structure of LEDs and reducing the p-side electron leakage at high current densities can the EQE efficiency droop problem be fundamentally solved.

3.6. *Impact of defects on carrier injection*

To elucidate the size effect on the efficiency of red LEDs, we calculate the electron and hole concentration distributions within the MQW in both models in Fig. 6. Taking the first quantum well near the p-side as an example, in Model 2, the electron concentration of LED V decreases by 23.5% and the hole concentration by 15.4%; the electron concentration of LED I decreases by 28% and the hole concentration by 24.6%; the presence of sidewall defects is responsible for this., which causes some of the electrons and holes at the edges of the light-emitting surface to be trapped by the defects, thus reducing the electron and hole concentrations in the MQW. The electron and hole concentrations in the MQW decrease more because the improved current distribution of the small-sized LED allows electrons and holes to reach the edge of the light-emitting surface, which the sidewall defects will eventually capture.

3.7. *Impact of defects on recombination rate*

Since the sidewall defect is located at the edge of the light-emitting surface, we calculate the horizontal electron and hole distributions in the first quantum well near the p-side for different model LEDs. In general, the carrier concentration in this quantum well is the highest among all quantum wells. As shown in Fig. 7, current crowding occurs below the n-electrode, and the carrier concentration gradually reduces as one moves away from the n-electrode. In Model 2, the sidewall defect region significantly reduces the holes and electrons. For example, the reduced levels of electron concentration at the edges of LED I, II, and V light-emitting surfaces are 27.6%, 22.1%, and 19.6%, and the reduced levels of hole concentration are 24.3%, 18.7%, and 16.6%, respectively. In addition, Fig. 7(c-f) in the calculation of different devices MQW in the horizontal radiative recombination rate and SRH non-radiative recombination rate distribution,

Optics EXPRESS

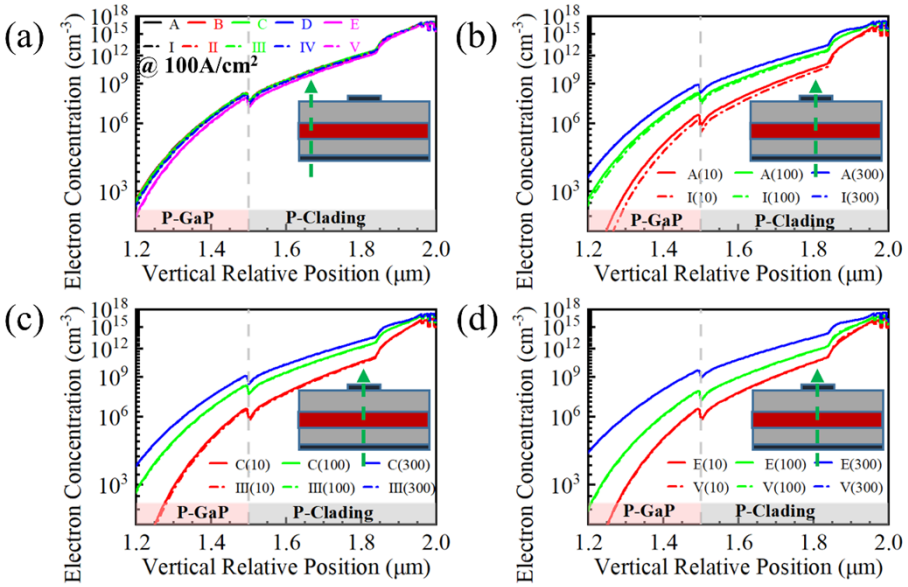

Fig. 5. (a) Vertical electron concentration distribution in the p-cladding layer and p-GaP layer at 2.5 μm from the edge of the light-emitting surface at an average current density of about 100 A/cm^2 for different LEDs in Models 1 and 2, and (b-d) vertical electron concentration distribution in the p-cladding layer and p-GaP layer at the center of the light-emitting surface at different average current densities for LED A, LED I, LED C, LED III, LED E and LED V. The inset shows the electron concentration distribution variation with the corresponding position (indicated by the green arrow).

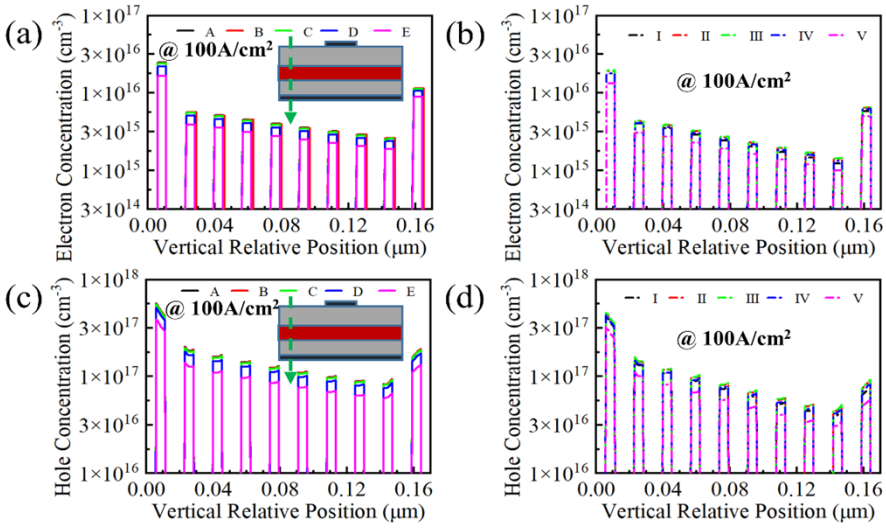

Fig. 6. (a-b) Vertical electron concentration distribution in the MQW region and (c-d) vertical hole concentration distribution in the MQW region for different LEDs in Model 1 and Model 2 at an average current density of about 100 A/cm^2 at 2.5 μm at the edge of the light-emitting surface. The inset shows the carrier concentration distribution variation with the corresponding position (indicated by the green arrow).

Optics EXPRESS

it can be seen that the light-emitting surface edge area of the radiative recombination rate and non-radiative recombination rate with the decreasing size increases. In Model 2, for LED V, the radiative recombination rate at the edge of the light-emitting surface is reduced by 24.9%, and the SRH recombination rate is reduced by 19.5%; for LED II, the radiative recombination rate at the edge of the light-emitting surface is reduced by 27.3%, and the SRH recombination rate is reduced by 21.9%; for LED I, the radiative recombination rate at the edge of the light-emitting surface is reduced by 33.7%, and the SRH recombination rate is reduced by 27.4%; this indicates that sidewall defects increase the SRH non-radiative recombination ratio at the edge of the light-emitting surface, leading to a decrease in EQE [39]. The smaller the LED size, the more significant the proportion of sidewall defects and the more severe the EQE reduction.

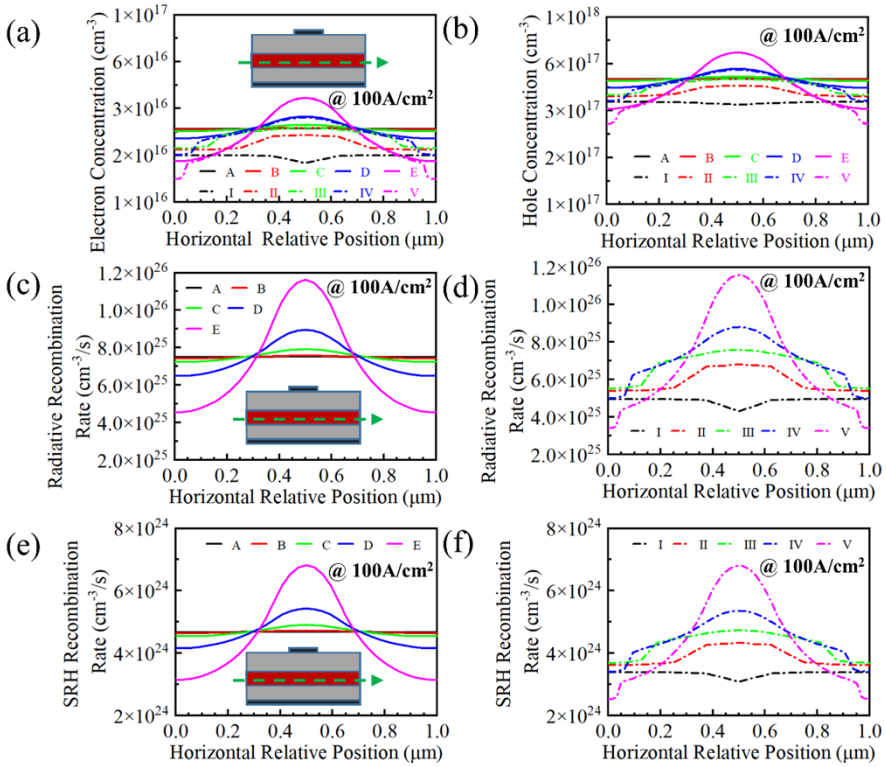

Fig. 7. (a) Horizontal electron concentration distribution, (b) horizontal hole distribution, (c-d) horizontal radiative recombination rate distribution, and (e-f) horizontal SRH recombination rate distribution in the first quantum well closest to the p-cladding layer for different LEDs in Model 1 and Model 2 at an average current density of about 100 A/cm^2. The inset shows the carrier concentration and recombination rate distribution variation with the corresponding position (indicated by the green arrow).

In summary, without considering sidewall defects, LEDs have improved EQE with decreasing chip size, owing to the enhanced current spreading effect of the smaller chip size. EQE and optical power density fall sharply with reducing device size when sidewall defects are considered, consistent with previous experimental reports [22]. Most importantly, we reveal a recombination mechanism in which sidewall defects cause an increase in the SRH recombination ratio, leading to a decrease in the peak EQE. In contrast, sidewall defects lead to a worse carrier injection efficiency, resulting in more current leakage and, thus, a more severe self-heating effect. In addition, our results show that p-side electron leakage at high current density is the root cause of

Optics EXPRESS

the efficiency droop of red LEDs and the more significant effect of temperature on the overall efficiency degradation of the LEDs.

4. Conclusions

In brief, we have demonstrated the effect of sidewall defects on the EQE, optical power density, self-heating effect, carrier concentration distribution, and recombination rate of red LEDs through a coupled electro-optical-thermal model, and the results are in good agreement with previous experimental data [22]. For GaN-based and AlGaInP-based LEDs, Wong et al. [18,40–42] demonstrated that even after trying different passivation methods on the etched sidewalls, the surface defects generated during etching could not be avoided entirely. Therefore, the effect of sidewall defects cannot be ignored when modeling LEDs. In addition, apart from the size effect caused by sidewall defects, the temperature significantly impacts the overall efficiency of the LED, so red LEDs should be avoided when operating in high-temperature environments as much as possible. When considering the self-heating effect of LEDs, the ohmic contact of LEDs should be optimized to improve the thermal performance of LEDs and avoid operating at high current densities as much as possible.

Funding. National Key Research and Development Program of China (2022YFB3604702).

Disclosures. The authors declare no conflicts of interest.

Data availability. Data underlying the results presented in this paper are not publicly available at this time but may be obtained from the authors upon reasonable request.

References

1. Y. Huang, G. Tan, F. Gou, M. C. Li, S. L. Lee, and S. T. Wu, "Prospects and challenges of mini-LED and micro-LED displays," J. Soc. Inf. Disp. **27**, 387–401 (2019).
2. D. W. Kim, S. W. Kim, G. Lee, J. Yoon, S. Kim, J.-H. Hong, S.-C. Jo, and U. Jeong, "Fabrication of practical deformable displays: advances and challenges," Light: Sci. Appl. **12**(1), 61 (2023).
3. K. Zhang, D. Peng, W. C. Chong, K. M. Lau, and Z. Liu, "Investigation of Photon-Generated Leakage Current for High-Performance Active Matrix Micro-LED Displays," IEEE T. Electron Dev. **63**(12), 4832–4838 (2016).
4. M. T. Vijjapu, M. E. Fouda, A. Agambayev, C. H. Kang, C.-H. Lin, B. S. Ooi, J.-H. He, A. M. Eltawil, and K. N. Salama, "A flexible capacitive photoreceptor for the biomimetic retina," Light: Sci. Appl. **11**(1), 3 (2022).
5. S. Ju, Y. Zhu, H. Hu, Y. Liu, Z. Xu, J. Zheng, C. Mao, Y. Yu, K. Yang, L. Lin, T. Guo, and F. Li, "Dual-function perovskite light-emitting/sensing devices for optical interactive display," Light: Sci. Appl. **11**(1), 331 (2022).
6. Z. Liu, W. C. Chong, K. M. Wong, and K. M. Lau, "GaN-based LED micro-displays for wearable applications," Microelectron. Eng. **148**, 98–103 (2015).
7. J. Xiong, E. Hsiang, Z. He, T. Zhan, and S. Wu, "Augmented reality and virtual reality displays: emerging technologies and future perspectives," Light: Sci. Appl. **10**(1), 216 (2021).
8. Y. Lin, Y. Lu, W. Guo, C.-F. Lee, S.-W. Huang Chen, H.-C. Kuo, S. Liang, C.-W. Sher, T. Wu, and Z. Chen, "Mini-LED and Micro-LED: Promising Candidates for the Next Generation Display Technology," Appl. Sci. **8**(9), 1557 (2018).
9. K. Rae, P. P. Manousiadis, M. S. Islim, L. Yin, J. Carreira, J. J. D. Mckendry, B. Guilhabert, I. D. W. Samuel, G. A. Turnbull, N. Laurand, H. Haas, and M. D. Dawson, "Transfer-printed micro-LED and polymer-based transceiver for visible light communications," Opt. Express **26**(24), 31474–31483 (2018).
10. A. Minotto, P. A. Haigh, L. G. Lukasiewicz, E. Lunedei, D. T. Gryko, I. Darwazeh, and F. Cacialli, "Visible light communication with efficient far-red/near-infrared polymer light-emitting diodes," Light: Sci. Appl. **9**(1), 70 (2020).
11. F. Olivier, S. Tirano, L. Dupré, B. Aventurier, C. Largeron, and F. Templier, "Influence of size-reduction on the performances of GaN-based micro-LEDs for display application," J. Lumin. **191**, 112–116 (2017).
12. M. S. Wong, J. A. Kearns, C. Lee, J. M. Smith, C. Lynsky, G. Lheureux, H. Choi, J. Kim, C. Kim, S. Nakamura, J. S. Speck, and S. P. DenBaars, "Improved performance of AlGaInP red micro-light-emitting diodes with sidewall treatments," Opt. Express **28**(4), 5787–5793 (2020).
13. H. E. Lee, S. H. Lee, M. Jeong, J. H. Shin, Y. Ahn, D. Kim, S. H. Oh, S. H. Yun, and K. J. Lee, "Trichogenic photostimulation using monolithic flexible vertical AlGaInP light-emitting diodes," ACS Nano **12**(9), 9587–9595 (2018).
14. J.-T. Oh, S.-Y. Lee, Y.-T. Moon, J. H. Moon, S. Park, K. Y. Hong, K. Y. Song, C. Oh, J.-I. Shim, H.-H. Jeong, J.-O. Song, H. Amano, and T.-Y. Seong, "Light output performance of red AlGaInP-based light emitting diodes with different chip geometries and structures," Opt. Express **26**(9), 11194 (2018).
15. Y. Zhao, J. Liang, Q. Zeng, Y. Li, P. Li, K. Fan, W. Sun, J. Lv, Y. Qin, Q. Wang, J. Tao, and W. Wang, "2000 PPI silicon-based AlGaInP red micro-LED arrays fabricated via wafer bonding and epilayer lift-off," Opt. Express **29**(13), 20217–20228 (2021).

Optics EXPRESS

16. J. Kou, C.-C. Shen, H. Shao, J. Che, X. Hou, C. Chu, K. Tian, Y. Zhang, Z.-H. Zhang, and H.-C. Kuo, "Impact of the surface recombination on InGaN / GaN-based blue micro-light emitting diodes," Opt. Express **27**(12), A643–653 (2019).
17. S. Hang, G. Zhang, C. Chu, Y. Zhang, Q. Zheng, Q. Li, and Z.-H. Zhang, "On the impact of the beveled mesa for GaN-based micro-light emitting diodes: electrical and optical properties," Opt. Express **30**(21), 37675 (2022).
18. M. S. Wong, R. C. White, S. Gee, T. Tanay, S. Gandrothula, H. Choi, S. Nakamura, J. S. Speck, and S. P. Denbaars, "Recovering the efficiency of AlGaInP red micro-LEDs using sidewall treatments," Appl. Phys. Express **16**(6), 066503 (2023).
19. C.-H. Oh, J.-I. Shim, and D.-S. Shin, "Current-and temperature-dependent efficiency droops in InGaN-based blue and AlGaInP-based red light-emitting diodes," J. Appl. Phys. **58**(SC), SCCC08 (2019).
20. K. A. Bulashevich and S. Y. Karpov, "Impact of surface recombination on efficiency of III-nitride light-emitting diodes," Phys. Status Solidi RRL **10**(6), 480–484 (2016).
21. M. V. Bogdanov, K. A. Bulashevich, I. Y. Evstratov, A. I. Zhmakin, and S. Y. Karpov, "Coupled modeling of current spreading, thermal effects and light extraction in III-nitride light-emitting diodes," Semicond. Sci. Technol. **23**(12), 125023 (2008).
22. K. Fan, J. Tao, Y. Zhao, P. Li, W. Sun, L. Zhu, J. Lv, Y. Quin, Q. Wang, J. Liang, and W. Wang, "Size effects of AlGaInP red vertical micro-LEDs on silicon substrate," Results Phys. **36**(105449), 105449 (2022).
23. R. H. Horng, H. Y. Chien, K. Y. Chen, W. Y. Tseng, Y. T. Tsai, and F. G. Tarn Tair, "Development and fabrication of AlGaInP-based flip-chip micro-LEDs," IEEE J. Electron Devices Soc. **6**, 475–479 (2018).
24. I. Vurgaftman, J. R. Meyer, and L. R. Ram-Mohan, "Band parameters for III–V compound semiconductors and their alloys," J. Appl. Phys. **89**(11), 5815–5875 (2001).
25. H. Kato, S. Adachi, H. Nakanishi, and K. Ohtsuka, "Optical properties of (AlxGa1−x)0.5In0.5P quaternary alloys," J. Appl. Phys. **33**(1R), 186 (1994).
26. D. Kressner, "A block Newton method for nonlinear eigenvalue problems," Numer. Math. **114**(2), 355–372 (2009).
27. D. A. Neamen, "Semiconductor Physics and Devices Basic Principles," Richard D. Irwin Inc. ISBN 0-256-0B405-X, 1992, Homewood IL 60430 (1992).
28. L. Gelczuk and M. Dabrowska-Szata, "Modification of energy bandgap in lattice mismatched InGaAs/GaAs heterostructures," Opt. Appl. **39**, 845 (2009).
29. P. Kaminski, M. Pawlowski, R. Kozlowski, and R. Ćwirko., and M. Palczewska, "High-resolution PITS studies of deep-level defects in semi-insulating GaAs and InP," Solid State Crystals: Growth and Characterization. SPIE. **3178**, 246–250 (1997).
30. S. C. Huang, H. Li, Z. H. Zhang, H. Chen, S. C. Wang, and T. C. Lu, "Superior characteristics of microscale light emitting diodes through tightly lateral oxide-confined scheme," Appl. Phys. Lett. **110**(2), 021108 (2017).
31. B. Fan, X. Zhao, J. Zhang, Y. Sun, H. Yang, L. J. Guo, and S. Zhou, "Monolithically Integrating III-Nitride Quantum Structure for Full-Spectrum White LED via Bandgap Engineering Heteroepitaxial Growth," Laser Photonics Rev. **17**(3), 2200455 (2023).
32. S. Zhou, X. Liu, H. Yan, Z. Chen, Y. Liu, and S. Liu, "Highly efficient GaN-based high-power flip-chip light-emitting diodes," Opt. Express **27**(12), A669–A692 (2019).
33. H. Hu, B. Tang, H. Wan, H. Sun, S. Zhou, J. Dai, C. Chen, S. Liu, and L. J. Guo, "Boosted ultraviolet electroluminescence of InGaN/AlGaN quantum structures grown on high-index contrast patterned sapphire with silica array," Nano Energy **69**, 104427 (2020).
34. S. Zhou, Z. Wan, Y. Lei, B. Tang, G. Tao, P. Du, and X. Zhao, "InGaN quantum well with gradually varying indium content for high-efficiency GaN-based green light-emitting diodes," Opt. Lett. **47**(5), 1291–1294 (2022).
35. S. S. Konoplev, K. A. Bulashevich, and S. Y. Karpov, "From large-size to micro-LEDs: scaling trends revealed by modeling," Phys. Status Solidi **1700508**, 1700508 (2018).
36. S. Lu, Y. Zhang, Z.-H. Zhang, P. C. Tsai, X. Zhang, S. T. Tan, and H. V. Demirl, "Strain-Reduced Micro-LEDs Grown Directly Using Partitioned Growth," Front. Chem. **9**, 639023 (2021).
37. C. Y. Lee, J. Y. Su, and C. M. Kuo, "630-nm n-type modulation-doped AlGaInP-AlInP multiquantum-well light-emitting diode," IEEE Photonics Technol. Lett. **18**, 25–27 (2006).
38. J. Cho, E. F. Schubert, and J. K. Kim, "Efficiency droop in light-emitting diodes: Challenges and countermeasures: Efficiency droop in light-emitting diodes: Challenges and countermeasures," Laser Photonics Rev. **7**(3), 408–421 (2013).
39. F. Olivier, A. Daami, C. Licitra, and F. Templier, "Shockley-Read-Hall and Auger non-radiative recombination in GaN based LEDs: a size effect study," Appl. Phys. Lett. **111**(2), 022104 (2017).
40. M. S. Wong, D. Hwang, A. I. Alhassan, C. Lee, R. Ley, S. Nakamura, and S. P. DenBaars, "High Efficiency of III-Nitride Micro-Light-Emitting Diodes by Sidewall Passivation Using Atomic Layer Deposition," Opt. Express **26**(16), 21324–21331 (2018).
41. Z. Zhu, T. Tao, B. Liu, T. Zhi, Y. Chen, J. Yu, D. Jiang, F Xu, Y Sang, Y. Yan, Z. Xie, and R. Zhang, "Improved Optical and Electrical Characteristics of GaN-Based Micro-LEDs by Optimized Sidewall Passivation," Micromachines **14**(1), 10 (2022).
42. J.-H. Park, M. Pristovsek, W. Cai, H. Cheong, C.-M. Kang, D.-S. Lee, T.-Y. Seong, and H. Amano, "Impact of Sidewall Conditions on Internal Quantum Efficiency and Light Extraction Efficiency of Micro-LEDs," Adv. Opt. Mater. **11**(10), 2203128 (2023).